Journal of Membrane Science 740 (2026) 124884

Contents lists available at ScienceDirect

Journal of Membrane Science

journal homepage: www.elsevier.com/locate/memsci

Neutron transmission studies with $GdCl_3$ for tracing concentration polarization in reverse osmosis

Vitaliy Pipich [a], Thomas Starc [b], Winfried Petry [c], Yoram Oren [d,*], Dietmar Schwahn [b,**]

[a] Jülich Centre for Neutron Science (JCNS) at Heinz Maier-Leibnitz-Zentrum (MLZ), Forschungszentrum Jülich GmbH, D-85747, Garching, Germany
[b] JCNS-1/ICS-1: Neutron Scattering and Soft Matter, Forschungszentrum Jülich GmbH, D-52425, Jülich, Germany
[c] Heinz Maier-Leibnitz-Zentrum (MLZ), Technische Universität München, Lichtenbergstr. 1, D-85748, Garching, Germany
[d] Zuckerberg Institute for Water Research, Jacob Blaustein Institutes for Desert Research, Ben-Gurion University of the Negev, Sede Boqer Campus, 84990, Israel

ARTICLE INFO

Keywords:
Reverse osmosis
Concentration polarization
Gadolinium chloride
Neutron transmission
Permeate flux

ABSTRACT

Concentration polarization (CP) is determined by neutron transmission in a reverse osmosis (RO) system consisting of two cells, one with and the other without an RO membrane, to get the net neutron response for the feed solution in front and far from the membrane separately. The aqueous feed was a dilute solution of NaCl and $GdCl_3$. The special feature of these experiments is that $GdCl_3$ can be selectively determined with neutrons, since the neutron absorption cross-section of Gd is larger orders of magnitude compared to other elements such as Na, Cl, and water, and therefore has a strong influence on the overall transparency of the sample for neutrons. It is therefore the transmission of neutrons through both cells (one with and the other without membrane), by which the concentration and CP of $GdCl_3$ can be determined. Transmission and small-angle scattering (SANS) were measured in parallel, demonstrating the performance of this method as an in-situ method for determining CP as a function of time under near-realistic conditions. The neutron experiments are complemented by measurements of permeate flux and electrical conductivity of the feed, which were used to determine the salt concentrations, the osmotic pressure and the concentration polarization of the two salts individually and of a mixture of both. The CP results of this study are in good agreement with the values presented in the literature, determined mainly from flux data under a wide variety of conditions.

1. Introduction

Reverse osmosis (RO) is a widely used technology to produce water for domestic applications from sea and brackish water and water recovery from wastewater [1,2]. The optimization of the process is still a subject of intensive research. A major approach is the search for the causes of fouling and scaling of the membrane surface and methods for their prevention, which can significantly affect the transmembrane flux and thus, the economic efficiency of the process [3].

Concentration polarization (CP) is a phenomenon resulting from the accumulation of dissolved and partially permeable components at the solution-membrane interface, that are driven to the feed side of the membrane surface by the permeate flux. CP results in increased energy demand for attaining a desired permeate flux and may enhance scaling and fouling by the increased concentration of the associated solutes. Monitoring the concentration profile in reverse osmosis (RO) and nanofiltration (NF) systems is challenging. In a recent review [4] the authors discuss the different techniques that have been used for observing CP. Among these, Raman Spectroscopy [5], Holographic Interferometry [6] and Laser-Induced Fluorescence [7] are listed for the optical methods while NMR [8] and Electrochemical Impedance spectroscopies are mentioned for non-optical methods. While the last technique has been used so far for ion exchange membranes, it is mentioned as relevant also for pressure driven processes. In another article [9], Neutron Radiography is used for determining concentration profiles on the two sides of a forward osmosis (FO) membrane.

In this study, we take advantage of the strong absorption cross-section of Gd ions to neutrons in an aqueous solution of $GdCl_3$ and NaCl, to follow the increase in concentration adjacent to a RO membrane due to CP using the transmission of thermal neutrons. This approach, demonstrated here for the first time, enables non-destructive operando transmission and SANS (small-angle neutron scattering) experiments to determine the average $GdCl_3$ concentration far and near the feed side of a RO membrane. The crossflow high-pressure setup

* Corresponding author.
** Corresponding author.
E-mail addresses: yoramo@bgu.ac.il (Y. Oren), d.schwahn@fz-juelich.de (D. Schwahn).

https://doi.org/10.1016/j.memsci.2025.124884
Received 2 June 2025; Received in revised form 26 October 2025; Accepted 29 October 2025
Available online 13 November 2025

required for operando neutron transmission RO experiments is described in detail in our previous publication [10]. The neutron transmission coefficient (T) is determined by following the attenuation of the neutron beam by the sample. The transmission of feed and membrane is dominated by the macroscopic absorption cross-section Σ_{abs} of Gd [11] from which the average $GdCl_3$ volume fraction of the feed in front and far from the membrane can be determined and thus obtaining an average CP at different conditions.

At this point it should be noted that the method of Neutron Radiography described in Ref. [9] fits well with the case of FO where the requirement for high concentrations in the draw-solution is crucial. The high LiCl concentration used in Ref. [9] is a tradeoff for its low cross-section for neutron absorption which is ~50 times less than for $GdCl_3$. Due to its limited solubility, $GdCl_3$ could not be used for FO purposes but fits well for RO as in this study. However, the main difference between the two studies is that in Ref. [9] transmission is measured in slices parallel to the membrane surface and thus the concentrations are averaged accordingly, while in this study this is currently done perpendicular to the membrane surface. In this paper, the term "transmission" refers to cross-membrane neutron propagation perpendicular to the membrane surface.

This article is structured as follows: In the main part, the $GdCl_3$ concentration is determined for increasing pressures in the range of 2–27 bar at a constant crossflow, followed by the application of varying crossflows up to 18 L/h at a constant pressure. Parallel to the neutron absorption measurements, the permeate flux (J_W) and the specific electrical conductivity (κ) of the membrane-far feed were determined. Both parameters are relevant auxiliary quantities to the neutron measurements. Complementary experimental data of permeate flux, electric conductivity (partly without neutrons) and transmission are given in Appendix A and B, whereas Appendix C presents data on relevant parameters used for the analysis of neutron transmission and permeate flux.

2. Experimental and methods

2.1. Neutron transmission and operando equipment

Transmission experiments were performed at the KWS3 instrument for very-small neutron scattering angles (VSANS) operated at the Heinz Maier-Leibnitz Zentrum (MLZ), Garching, Germany [12]. KWS3 covers a

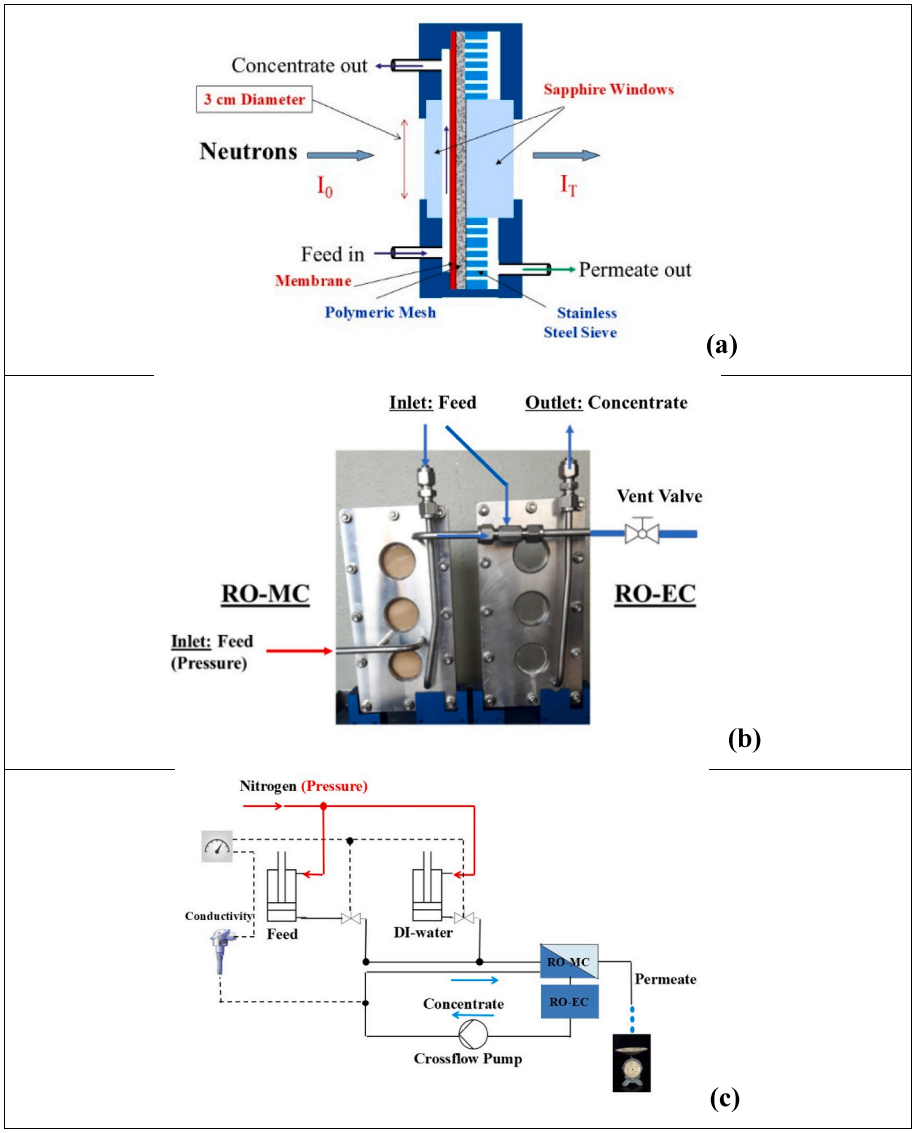

Fig. 1. (a) Schematic view of RO-MC, showing the neutrons pathway. **(b)** Photo of the RO-MC and RO-EC cells as used in the desalination experiments. The transmission experiments were conducted exclusively in the central sapphire window. **(c)** Flow diagram of the system for delivering the feed to RO-MC and RO-EC cells at fixed pressure and crossflow while maintaining a constant feed composition. The solid and dashed lines represent stainless steel pipes for the supply solutions and lines for electrical connections, respectively.

range of the scattering vector $|\underline{Q}|$ between 10^{-4} and 2.5×10^{-3} Å^{-1} allowing the analysis of scattering particles in the μm range [13]. The equipment and the functioning of the operando experiments are described in detail in Ref. [10]. Fig. 1(a) shows the design of the neutron transmission pressure cell which includes the RO-TFC membrane, the supporting mesh at the permeate side and sapphire windows that are fully transparent for neutrons. This cell is hereinafter referred to as RO-MC. A second pressure cell of identical design but without membrane and spacer (designated hereinafter RO-EC) is connected in series to the feed circuit of RO-MC. In this way, we can determine salt concentrations of the feed near the membrane surface and in the bulk solution, from which CP can be determined. Fig. 1 (b) shows a photo of the RO-MC and RO-EC cells as used in the desalination experiments. Fig. 1 (c) also shows the setup of feed delivery to RO-MC and RO-EC at constant pressure or crossflow. The feed solution is circulated by a crossflow pump. The electrical conductivity (EC) of the feed provides information about the bulk salt concentration but also serves for controlling the operation of two valves for pushing the deionized water and the feed solution pistons, to ensure constant feed concentration. This control process is necessary because salt-free water is permanently lost from the feed solution due to permeation through the membrane [10].

Each pressure cell is equipped with three pairs of sapphire windows for neutron transmission [15]. Only the middle window was used in this study, thus determining the neutron transmission in the central section of the membrane, where the fully developed flow is expected. The $GdCl_3$ concentration was determined within the 1.5×1.5 cm^2 neutron beam cross-section, located at the center of the total membrane area of 4.5×13.7 cm^2 = 61.7 cm^2. The beam area is determined by an aperture made of neutron absorbing material in front of a RO cell. The $GdCl_3$ concentration is determined from the ratio of the neutron intensity I_T behind the sample and the incident intensity I_0 according to $T = I_T/I_0$, as shown schematically in Fig. 1(a). Since the absorption of thermal neutrons increases with λ, a particular long wavelength of λ = 12.8 Å was used for all neutron measurements [11].

2.2. Membrane and feed solutions

The membrane used in this study is the RO98 pH t by Alfa Laval (Lund, Sweden). All measurements started with compaction of a pristine membrane sample whose pore structure was characterized in previous SANS experiments [14–16]. The experiments were done with deionized water (DI-H_2O) as well as with a solution containing 1.06 g/L $GdCl_3$ and 4.69 g/L NaCl. The neutron experiments were mainly carried out with 18 L/h crossflow and trans membrane pressures up to 27 bar.

2.3. Determination of $GdCl_3$ concentration by neutron transmission

The neutron transmission coefficient (T) is the relevant parameter for determining the salt concentration in the feed. The transmission is determined by the macroscopic cross-section of the feed Σ (salt solution or H_2O) and the cell depth d_S according to Eq. (1). It should be noted that the cell depth, d_S, changes under applied pressure due to the construction material's elasticity. Albeit small, these changes can be detected by neutron transmission when salt-free D_2O is used. The variation of d_S with pressure is presented in Figure C1(a) and has been considered in the evaluation of the transmission measurements. In the RO-EC with the thickness d_S the macroscopic cross-sections of water $\Sigma_{H_2O} = -\ln(T_{H_2O})/d_S$ is calculated directly from the water transmission T_{H_2O}, whereas the Σ_{NaCl} and Σ_{GdCl_3} were evaluated from the absorption cross-sections for the neutron wavelength of λ = 12.8 Å [11] as compiled in Table C1. The transmission ratio of the salt solution relative to pure water $T_{GdCl_3-H_2O}/T_{H_2O}$ delivers the $GdCl_3$ volume fraction Φ as shown in Eq. (2). In case of the RO-MC cell we also must consider $\Sigma_M = \Sigma_{Mem} + \Sigma_{Spacer}$, i.e. the macroscopic cross-sections of membrane and spacer according to $-\ln(T_{MC-GdCl_3-H_2O}) = d_M \times \Sigma_M + (d_S - d_M) \times \{\Phi \times \Sigma_{GdCl_3} + (1-\Phi) \times \Sigma_{H_2O}\}$. The ratio of $T_{MC-GdCl_3-H_2O}/T_{MC-H_2O}$ results in Eq. (3), considering the membrane plus spacer thickness (d_M = 0.058 cm), which corresponds to a feed channel height of $\Delta d_S = (d_S - d_M)$ (Figure C1(c)). The neutron transmission of membrane plus spacer, expressed as $T_M = \exp(-\Sigma_M \times d_M)$, is eliminated by the ratio of $(T_{MC-GdCl_3-H_2O} \times T_M) / (T_{MC-H_2O} \times T_M)$ and does not affect the neutron transmission of the feeds, i.e., the degree of salinity in the same pressure cell (Eq. (3)). This procedure illustrates neutron transmission measurements: (i.) neutrons easily transmit through the sample and entire sample environment, thereby enabling operando experiments, (ii.) extraction of the pure signal of the salt solution is achieved by dividing the transmission of the entire cell filled with salt solution by the identical cell filled with DI-H_2O, (iii.) the transmission of the RO-MC and RO-EC are determined separately by independent measurements.

The calculated transmission ratios $T_{GdCl_3-H_2O}/T_{H_2O}$ of Eq. (2) are plotted in Fig. 2 as a function of $GdCl_3$ concentration. As mentioned above, the neutron path length through the cell (d_S) is affected by the applied pressure, which in turn influences the transmission ratio. This is shown in Fig. 2 for the RO-MC and RO-EC cells at ΔP = 0 and 27 bar, highlighting the sensitivity of neutron absorption at wavelength of 12.8 Å to the determination of $GdCl_3$ concentration. In these plots, the contribution of NaCl can be neglected as it is practically transparent to neutrons with a transmission of 0.998. The $GdCl_3$ concentration in Eq. (3) was determined by assuming zero $GdCl_3$ concentration in the membrane and spacer.

$$T = I_T / I_0 = \exp(-\Sigma \times d_S) \tag{1}$$

$$-\ln\left(T_{GdCl_3-H_2O} / T_{H_2O}\right) / d_S = \Phi \times \left(\Sigma_{GdCl_3} - \Sigma_{H_2O}\right) \simeq \Phi \times \Sigma_{GdCl_3} \tag{2}$$

$$-ln\left(T_{MC-GdCl_3-H_2O} / T_{MC-H_2O}\right) / (d_S - d_M) = \Phi \times \left(\Sigma_{GdCl_3} - \Sigma_{H_2O}\right) \simeq \Phi \times \Sigma_{GdCl_3} \tag{3}$$

3. Results of RO operando neutron transmission experiments

In this section, we investigate the pressure induced increase of $GdCl_3$ concentration at the solution-membrane interface, by following neutron

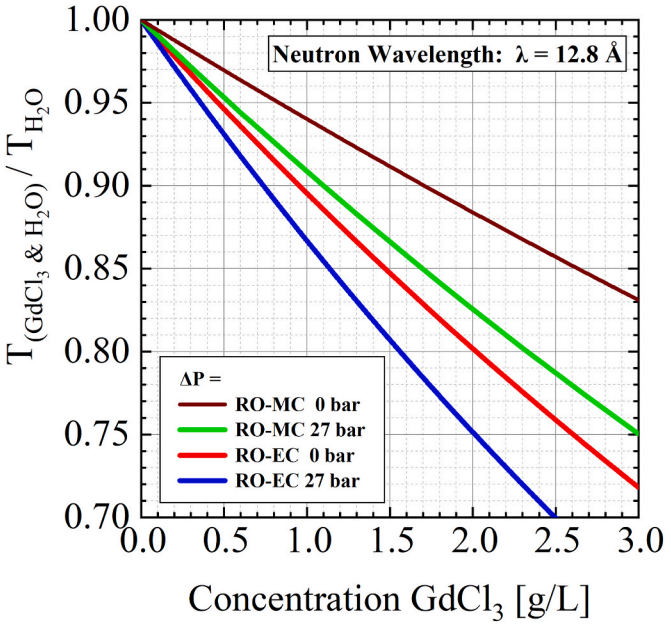

Fig. 2. Ratio of neutron transmissions vs. concentration of $GdCl_3$ in H_2O in the RO-EC and RO-MC cells of λ = 12.8 Å neutrons at ΔP = 0 and 27 bar (Eqs. (2) and (3)).

transmission in the RO-MC and RO-EC cells. Simultaneously, the permeate flux (J_w) and the electrical conductivity (κ) of the feed were measured. The time dependence of electrical conductivity, permeate flux, neutron transmission and scattering intensity ($d\Sigma/d\Omega(Q)$) is presented in Appendix A. These measurements were carried out over 21 and 37 h for salt-free water and salt solution, respectively, at $\Delta P = 27$ bar and crossflows of 18, 12 and 6 L/h.

3.1. Permeate flux and feed electrical conductivity

Fig. 3(a) and (b) show the permeate flux (J_W) and electrical conductivity (κ) of DI-H_2O and the salt solution as functions of transmembrane pressure, from which the water permeabilities were determined. The permeate flux was measured with a crossflow of 18 L/h, corresponding to a flow velocity of $v \simeq 9.4$ cm/s for the channel cross-section of 0.53 cm^2 at 27 bar, i.e. 4.5 cm channel width and 0.118 cm channel height above the membrane (Figure C1). Under these conditions, the Reynolds number ($Re \simeq 216$) supports the assumption of laminar flow (Appendix C4). In Fig. 3(b), a constant conductivity of (8.10 ± 0.07) mS/cm is measured for ΔP larger than 10 bar. The slight increase of κ in DI-H_2O results from small contamination possibly from the membrane as discussed in Ref. [15].

Fig. 3(a) shows a linear increase of the permeate flux with the *trans*-membrane pressure for DI-H_2O and the $GdCl_3$ + NaCl solution, in accordance with Eq. (4). According to Eq. (4), the permeate flux is proportional to the permeability (A) times the hydrostatic pressures ΔP and ΔP^* for the aqueous salt-free and salt solutions, respectively [17,18]. The osmotic pressure differences $\Delta\pi_f$ and $\Delta\pi_{mf}$ are defined as $\Delta\pi_f = (\pi_f - \pi_p)$ and $\Delta\pi_{mf} = (\pi_{mf} - \pi_p)$ with π_p the osmotic pressure on the permeate side. The osmotic pressure at the membrane surface $\Delta\pi_{mf}$ is determined from the difference of ΔP^* and ΔP between and at the same flux according to $J_W(\Delta P) = J_W(\Delta P^*)$, i.e. $\Delta\pi_{mf} = \Delta P^* - \Delta P$ as indicated by the green arrow in Fig. 3(a). CP is determined by the concentrations of the salts on the membrane surface in relation to the feed far from the membrane (section 3.2) and is determined by $CP = \Delta\pi_{mf} / \Delta\pi_f$ [17]. For quantitative analysis, the permeate fluxes of DI-H_2O and salt water in Fig. 3(a) were fitted using Eq. (4) obtaining the water permeabilities of $A^{H_2O} = (0.507 \pm 0.015)$ and $A^{salt} = (0.405 \pm 0.003)$ in units of L/(m^2 h bar), and the osmotic pressure of the feed $\Delta\pi_f = (2.19 \pm 0.15)$ bar determined at $J_W = 0$. At $J_W(\Delta P) = J_W(\Delta P^*)$ both pressures are related by $\Delta P^* = \Delta\pi_f + (A^{H_2O}/A^{Salt}) \times \Delta P$, which allows to express the osmotic pressure $\Delta\pi_{mf}$ and CP as function of ΔP^* in Eqs. (5) and (6). At $\Delta P^* = 27$ bar we determine the osmotic pressure $\Delta\pi_{mf} = (7.06 \pm 0.51)$ bar and a polarization factor of $CP = (3.24 \pm 0.31)$ (Fig. 7 and Table 1).

$$J_W = A^{H_2O} \times \Delta P \text{ and } J_W = A^{salt} \times (\Delta P^* - CP \times \Delta\pi_f) \quad (4)$$

$$\Delta\pi_{mf} = (A^{salt}/A^{H_2O}) \times \Delta\pi_f + (1 - A^{salt}/A^{H_2O}) \times \Delta P^* \quad (5)$$

$$CP = \Delta\pi_{mf}/\Delta\pi_f = (A^{salt}/A^{H_2O}) + \{(1 - A^{salt}/A^{H_2O}) / \Delta\pi_f\} \times \Delta P^* \quad (6)$$

3.2. Salt concentration and concentration polarization

A typical course of concentration c(x) of dissolved nonpermeable substances in RO is shown schematically in Fig. 4. Eq. (7) describes the diffusion and convection transport of salts at the membrane interface via mass balance [19]. $J_W\,\delta/D_s$ is the Peclet number and D_S/δ, the feed-side mass transfer coefficient, k_f. The CP of the salt is derived from the ratio of the salt concentrations at the membrane surface (c_{mf}) and of bulk (c_f), i.e. $CP = c_{mf}/c_f$ assuming c_f and $c_{mf} \gg c_p$. Typical values in the literature are in the range below 3, as shown in Section 4. At $\Delta P = 27$ bar, we determine for both salts a mass transfer coefficient $k_f = (2.41 \pm 0.19) \times 10^{-6}$ m/s from $CP = (3.24 \pm 0.31)$ (Fig. 7) and $J_W = (10.2 \pm 0.1)$ L/(m^2 h) (Fig. 3(a)). Using a diffusion coefficient D_S for salts in water at 25 °C, which is generally given in the range of 1.5×10^{-5} cm^2/s [19], we estimate a boundary layer thickness of (0.64 ± 0.05) mm as compiled data in Table 1. This implies a CP interface thickness occupying about 1/2 of the actual channel height.

$$J_W\,c(x) - D_s \times dc(x) \Big/ dx = J_W\,c_p \text{ and } \frac{c_{mf} - c_p}{c_f - c_p} \equiv \frac{\Delta c_{mf}}{\Delta c_f} = \exp(J_W\,\delta/D_s) \quad (7)$$

The variation of electrical conductivity (κ) in DI-H_2O and the salt solution with ΔP is shown in Fig. 3(b) as measured in the RO-EC cell. For DI-H_2O, a slight increase of κ in the range of μS/cm is observed, while κ for the $GdCl_3$ + NaCl solution shows ≃ 12 % increase between 0 and 10 bar and remains constant at $\kappa = (8.10 \pm 0.07)$ mS/cm for $\Delta P > 15$ bar (Table 1) and corresponds to (84 ± 5) % of the nominal $GdCl_3$ + NaCl concentration.

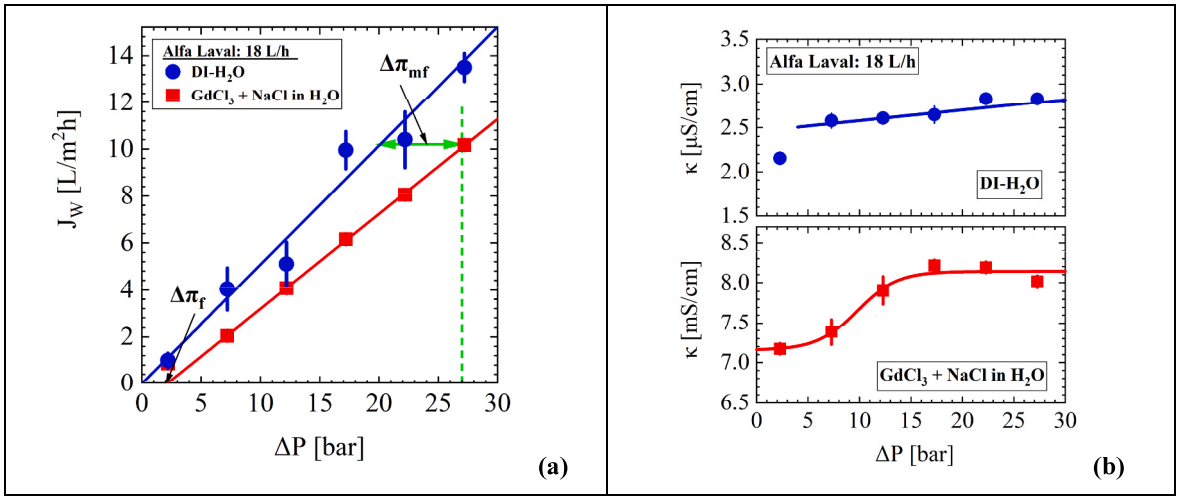

Fig. 3. (a) Permeate flux vs. pressure at crossflow of 18 L/h. The green double arrow indicates the osmotic pressure $\Delta\pi_{mf}(\Delta P)$ at 27 bar (Eq. (5)). The larger error bars for DI-H_2O are due to the availability of short beam time. **(b)** Corresponding electrical conductivity of DI-H_2O and $GdCl_3$ + NaCl solution vs. pressure.

Table 1
Permeate flux data accompanied by SANS experiments and control experiments without neutrons performed at constant crossflow of 18 L/h.

Parameter	Measurements with neutrons (27 bar)			Measurements without neutrons (24 bar)				
				Membrane sample 1		Membrane sample 2		
Feed	DI-H_2O	$GdCl_3$	$GdCl_3$+NaCl	DI-H_2O	$GdCl_3$	DI-H_2O	NaCl	$GdCl_3$ + NaCl
Nominal Concentration [g/L]	–	1.06	5.75	–	1.5	–	4.69	6.16
Conductivity κ [mS/cm]	$(2.7 \pm 0.1) \times 10^{-3}$	–	8.10 ± 0.07	$(2.85 \pm 0.06) \times 10^{-3}$	1.87 ± 0.03	$(2.85 \pm 0.06) \times 10^{-3}$	8.12 ± 0.06	9.98 ± 0.29
Measured Concentration [g/L]	–	1.05 ± 0.04	5.05 ± 0.06	–	1.64 ± 0.03	–	4.69 ± 0.04	6.33 ± 0.13
Permeability A [L/(m^2 h bar)]	0.507 ± 0.015	0.405 ± 0.003		1.64 ± 0.01	1.37 ± 0.03	2.71 ± 0.07	1.72 ± 0.05	1.43 ± 0.05
$\Delta\pi_f$ [bar]	–	–	2.19 ± 0.15	–	0.90 ± 0.12	–	1.95 ± 0.56	2.67 ± 0.24
$\Delta\pi_{mf}$ [bar]	–	–	7.06 ± 0.51	–	4.83 ± 0.62	–	10.7 ± 0.95	14.0 ± 1.1
J_W	13.5 ± 0.6	–	10.2 ± 0.1	40.2 ± 0.9	31.4 ± 0.2	62.5 ± 0.2	37.8 ± 0.1	31.4 ± 0.1
k_f [10^{-6} m/s]	–	–	2.41 ± 0.19	–	5.17 ± 0.61	–	6.19 ± 0.99	5.26 ± 0.64
δ [mm]	–	–	0.64 ± 0.05	0.29 ± 0.04	–	0.24 ± 0.04	0.29 ± 0.04	0.29 ± 0.04
CP	———	**1.97 ± 0.18**	**3.24 ± 0.31**	———	**5.39 ± 1.06**	———	**5.46 ± 1.50**	**5.24 ± 0.63**

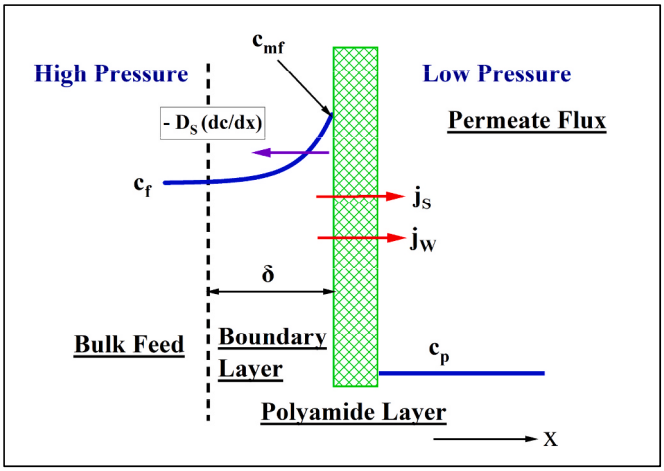

Fig. 4. Schematic view of salt concentration profiles at the RO membrane-solution interfaces showing salt CP. J_S and J_W are the permeate flux of the solutes and water, respectively.

3.3. Neutron transmission as a function of pressure and feed flux rate

In this section neutron transmission and flux measurements are analyzed. This will allow an independent determination of $GdCl_3$ concentration changes. Fig. 5(a) shows the neutron transmission data of DI-H_2O and the aqueous $GdCl_3$ + NaCl solution measured in the RO-EC and RO-MC cells as a function of hydrostatic pressure at a cross flow of 18 L/h. Fig. 5(b) shows the transmission at a constant pressure of 27 bar for an increasing crossflow rate. The transmission of salt solutions always shows smaller values compared to those for DI-H_2O due to the strong absorption cross-section of Gd towards neutrons. The transmissions in Fig. 5(b) show a change of about 2 % increase and decrease for the RO-MC and RO-EC, respectively, for a crossflow up to 18 L/h.

3.4. Concentration polarization of $GdCl_3$

The $GdCl_3$ concentrations determined from the neutron transmission data in Fig. 5(a) are shown in Fig. 6(a) as a function of the applied pressure for RO-EC and RO-MC. The average $GdCl_3$ concentration of the feed solution far from the membrane (i.e. in the RO-EC) is between 0.77 and 1.2 g/L in the given pressure range, which corresponds to a factor of 0.73–1.13 of the nominal $GdCl_3$ concentration of 1.06 g/L. These values show good agreement with a nominal $GdCl_3$ + NaCl concentration with a (16 ± 1) % lower value. The increase of κ from 7.15 to 8.10 mS/cm in

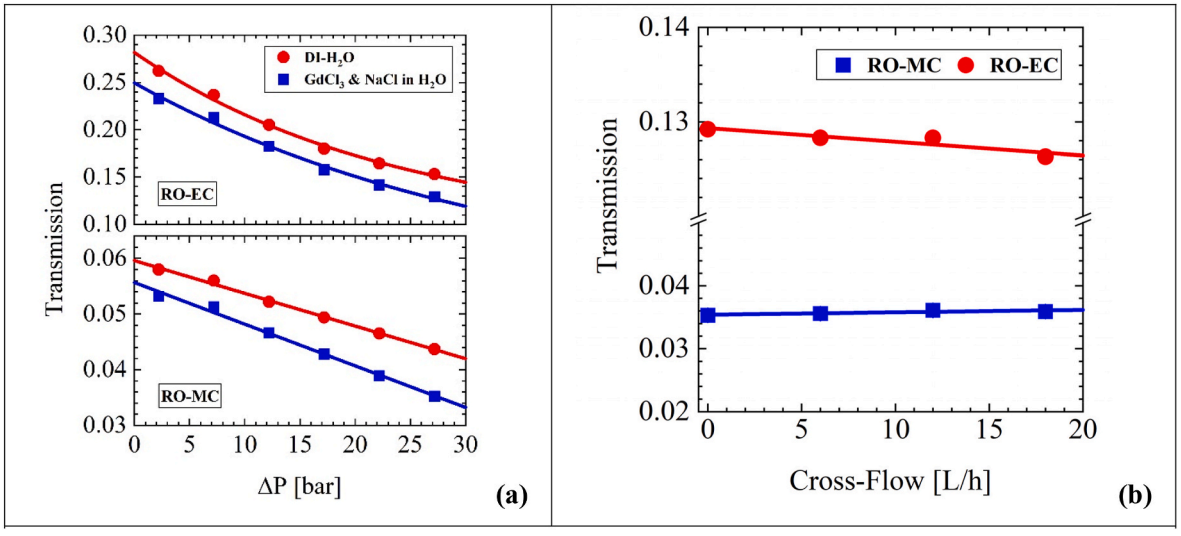

Fig. 5. Transmission data of DI-H_2O and Gd_3Cl + NaCl in H_2O for the RO-EC and RO-MC cells, **(a)** at crossflow of 18 L/h vs. pressure and **(b)** at constant hydrostatic pressure of 27 bar vs. crossflow. Transmission decreases with pressure due to the increase of the channel width with pressure.

Fig. 3(b) is accompanied by an increase in salt concentrations caused by the control of the operando apparatus (Fig. 1(c). The higher $GdCl_3$ concentration in the RO-MC cell near the membrane surface shows a significantly increasing $GdCl_3$ concentration from about 30 % to 91 % with increasing pressure from 2.2 to 27 bar, which corresponds to a CP increase of 1.3 to (1.91 ± 0.18).

4. Discussion and summary

In this work, neutron transmission was measured along with permeate flux and electrical conductivity of a two-component aqueous salt solution near and far from the membrane surface in real-time RO desalination experiments, to finally determine CP as a function of hydrostatic pressure. A $GdCl_3$ + NaCl solution was used as a feed, with the special feature that neutron transmission is sensitive only to the concentration of $GdCl_3$, while the permeate flux and electrical conductivity are affected by the total salt concentration. To determine the individual effect of each of the salts, we conducted a separate series of experiments with no neutron transmission involved. For that purpose a new RO98 pH t membrane sample was tested with solutions containing $GdCl_3$ and NaCl separately and as a mixture. The results are discussed below, and the relevant data are given in Appendix B.

The permeability (A) and osmotic pressure of the solutions ($\Delta\pi_f$) shown in Table 1 were determined from the flux rates (J_W) in Fig. 3(a) and B1 applying Eq. (4). At $J_W = 0$, $\Delta\pi_f$ was determined for the $GdCl_3$ and NaCl solutions in Figure B1(a) and (b) as well as for the $GdCl_3$ + NaCl solutions in Fig. 3(a) and B1(b), indicating a nominal $GdCl_3$ concentration of 1.06 (Fig. 3) and 1.5 g/L (Figure B1), respectively. The first mentioned concentration is close to the concentration derived from the neutron transmission measurements in Fig. 6(a). A third parameter for following the total concentration of the $GdCl_3$ + NaCl feed solution is the electrical conductivity (κ). The results from neutron experiments in Fig. 3(b) show a κ = (8.10 ± 0.07) mS/cm for the GdCl3 + NaCl solution at ΔP > 10 bar, which is about 16 % smaller than the value evaluated from the nominal concentrations shown in Appendix C.

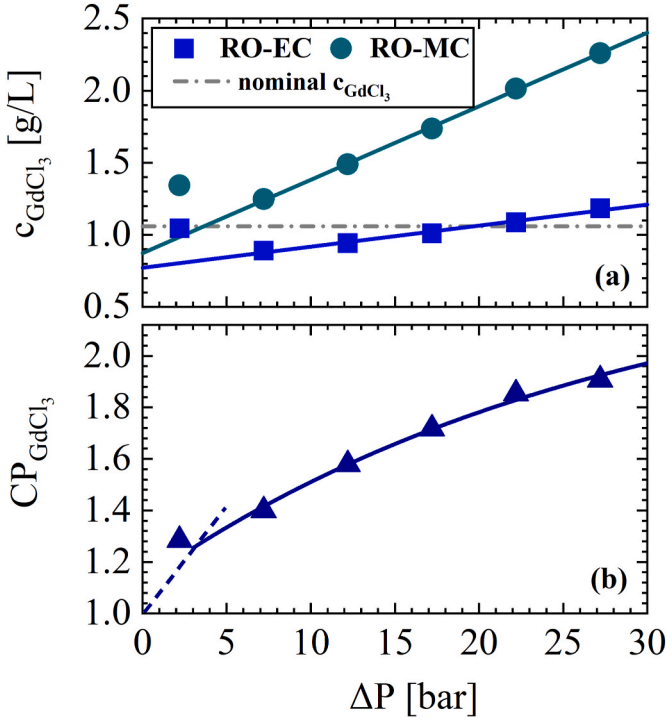

Fig. 6. **(a)** $GdCl_3$ concentration as a function of pressure determined from the transmission data of the RO-MC and RO-EC cells at a crossflow of 18 L/h. The nominal concentrations of $GdCl_3$ and NaCl are 1.06 g/L and 4.69 g/L, respectively. **(b)** CP for $GdCl_3$.

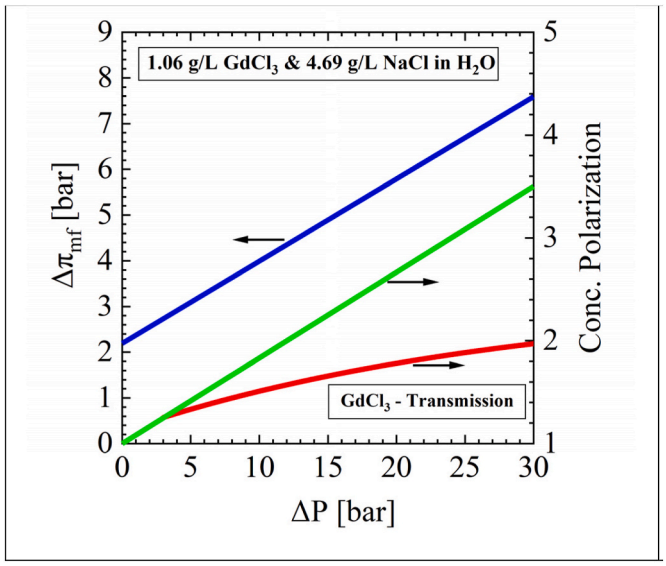

Fig. 7. Osmotic pressure $\Delta\pi_{mf}$ and CP versus pressure at CF = 18 L/h. Osmotic pressure (blue line) and CP (green line) of the $GdCl_3$ + NaCl mixture were determined from flux experiments (J_W), while the CP for $GdCl_3$ (red line) was determined from neutron transmission.

Fig. 7 shows the osmotic pressure and CP of the $GdCl_3$ + NaCl mixture as a function of ΔP, as obtained from the flux data (J_W) using Eq. (5). At ΔP = 27 bar, we find $\Delta\pi_{mf}$ = (7.06 ± 0.51) bar and CP = (3.24 ± 0.31) (Table 1). CP of $GdCl_3$ in Fig. 6(b) derived from the neutron transmission data and presented again for comparison, shows a continuous increase with pressure up to 56 % of the CP value of the two salts at ΔP = 27 bar. The values of $\Delta\pi_{mf}$ and CP from the flux experiments in Fig. 3(a) and B1, are depicted in Fig. 8 as a function of permeate flux as formulated in Eq. (8). The osmotic pressure ($\Delta\pi_f$) of the feed solution far from the membrane surface is determined at zero permeate flux and increases near the membrane surface ($\Delta\pi_{mf}$) with the hydrostatic pressure ΔP due to accumulation of salt molecules. The permeate flux of DI-H_2O and salt solution is described in good approximation in Eq. (4) [19]. The parameters of the permeabilities A^{H_2O} and A^{salt} as well as the osmotic pressure of the salt solutions $\Delta\pi_f$ are summarized in Table 1 for the SANS data and flux data. The permeate flux of the feed solution of the membrane used in the neutron transmission experiments, extrapolated to 24 bar, is about 9 L/(m^2 h), while the corresponding flux of membranes 2 is 31 L/(m^2 h) as shown in Fig. 3(a) and B1(b).

$$\Delta\pi_{mf}\left(J_W^{salt}\right) = \Delta\pi_f + \left[\left(1 / A^{salt} - 1 / A^{H_2O}\right)\right] \times J_W^{salt} \quad (8)$$

The channel width (d_S) in the center of the cell increases with pressure, which in turn has a strong influence on the flow velocity (Figure C1 (b)). In this context, the boundary thickness δ and CP at the membrane surface are affected (Fig. 4, Eq. (7), Table 1). The neutron transmission experiments show a δ = (0.64 ± 0.05) mm at ΔP = 27 bar (Table 1), which must be compared with the corresponding channel height $\delta 8 d_S$ = 1.18 mm (Figure C1). We found with $\delta/\Delta d_S \simeq 0.54$ a boundary thickness of about half the channel height. On the other hand, due to the larger permeate flux and CP of the corresponding $GdCl_3$ + NaCl flux experiment in Figure B1(b) (Table 1) a boundary thickness of δ = 0.29 ± 0.04) mm is derived at ΔP = 24 bar thus covering with $\delta/\Delta d_S \simeq 0.25$ only a quarter of the feed channel. These estimates provide an indication of the degree of averaging of salt concentration in determining CP.

Finally, we would like to look at other, published methods used for determining CP in RO systems. The challenge is that there are relatively few publications on this topic, and the measurements were carried out under different parameters. For a fair comparison, we have therefore

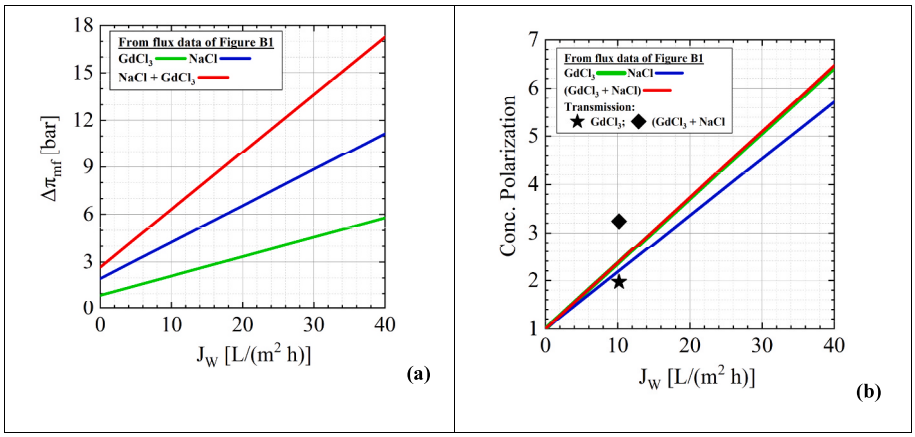

Fig. 8. **(a)** Osmotic pressure at the membrane surface versus permeate flux as determined from the flux data in Figure B1(a) and (b) (see also Table 1). **(b)** CP versus permeate flux. (Symbols: $GdCl_3$ (green line), NaCl (blue line), and ($GdCl_3$ + NaCl) (red line). The symbols (black star) and (black rhombus) represent the CP of $GdCl_3$ and $GdCl_3$ + NaCl as determined from neutron transmission and permeate flux (Fig. 3(a)) at ΔP = 27 bar (Table 1).

also indicated the parameters under which the work was carried out. In the introduction we already mentioned several articles [4–9]. Here we discuss the results of the following methods on a more quantitative basis. (i.) Digital Holographic Interferometry (DHI) visualized the shape of the CP layer of Na_2SO_4 and NaCl feed solutions showing a close relationship between permeate flux, polarization layer and crossflow velocity [6]. (ii.) In another study [20], CP was determined from permeate flux experiments for several aqueous feed solutions of NaCl, $MgCl_2$, $CaCl_3$, and Na_2SO_4 at the surface of a BW30XFR membrane. For example, the permeate flux of a 100 mM NaCl solution was determined for hydrodynamic pressures between 7 and 26 bar and a crossflow velocity of 1 gallon per minute. This very large crossflow of 227 L/h exhibits turbulent flow behavior (Reynolds number Re = 3220), in contrast to the neutron experiments performed with a maximum crossflow of 18 L/h (Re ≃ 216), which are clearly in the range of laminar flow. The authors determined a CP module between 1.1 and 1.8 depending linearly on permeate flux and corresponds to a pressure range between 7 and 26 bar. (iii.) Similar flow experiments were conducted in Ref. [21]. CP shows a time evolution of approximately 1.2–1.7 for two crossflow velocities of 4 and 11 cm/s. For two membranes (XLE and BW), a CP decrease from 1.8 to 1.6 and from 1.6 to 1.3 with increasing crossflow was measured. (iv.) In Ref. [22] the CP module based on numerical finite element model calculations is discussed. The local CP modulus of a $CaCl_2$ feed solution increases from about 1.3 to 2.6 with decreasing Reynolds number from 489 to 48.9.

The above-mentioned articles show a CP range of 1.0–2.6 for a wide range of conditions, which is in good agreement with the values determined by neutron transmission for $GdCl_3$ (Fig. 6). However, the CP values from our "no neutron" flux experiments of $GdCl_3$ + NaCl show a larger CP of around 6.5 for a permeate flux of 40 L/(m^2h) (Fig. 8). Similar permeate flux experiments in Ref. [22] show a significantly smaller CP between 1.5 and 1.8 for a hydrostatic pressure of 26 bar (corresponds to 80 L/(m^2h)), which, however, was subjected to much larger crossflow of 227 L/h with turbulent flow behavior.

There is no doubt that determining a CP profile perpendicular to the membrane surface would provide a more detailed view of the CP at the membrane-feed interface as was achieved from DHI in Ref. [6]. However, this lack of neutron transmission is offset by the determination of the quantitative salt concentration and CP under realistic RO conditions. The combination of neutron transmission, permeate flux and electrical conductivity is a particular strength of our method, as it allows a comprehensive analysis of CP formation under realistic wastewater desalination conditions.

CRediT authorship contribution statement

Vitaliy Pipich: Investigation, Formal analysis, Data curation. **Thomas Starc:** Investigation. **Winfried Petry:** Writing – review & editing, Visualization, Supervision, Conceptualization. **Yoram Oren:** Writing – review & editing, Visualization, Supervision, Investigation, Conceptualization. **Dietmar Schwahn:** Writing – review & editing, Writing – original draft, Validation, Methodology, Investigation, Formal analysis, Conceptualization.

Funding

No funding

Declaration of competing interest

The authors declare that they have no known competing financial interests or personal relationships that could have appeared to influence the work reported in this paper.

Acknowledgments

SANS experiments were performed at, respectively, the KWS3 and KWS1 at the Heinz Maier-Leibnitz Zentrum (MLZ), Garching, Germany. D.S. would like to thank Prof. Dr. Stephan Förster, head of the Jülich Center for Neutron Science (JCNS-1) and Institute for Complex systems (ICS-1) at the Forschungszentrum Jülich GmbH for his hospitality.

Nomenclature

Neutrons

T	Neutron transmission
$d\Sigma/d\Omega(Q)$	Differential macroscopic cross-section
Σ_{H2O}	Total macroscopic cross-section of H_2O
Σ_{abs}	Macroscopic absorption cross-section
$d\Sigma/d\Omega_{inc}$:	Incoherent scattering cross-section
Θ:	Scattering angle
λ	Wavelength of neutron
k	Wavenumber of neutron ($2\pi/\lambda$)
Q	Momentum transfer defined as $Q = 4\pi/\lambda \sin(\delta/2)$
Ω_M	Volume of molecule "M″
ρ_M	Coherent scattering length density of molecule "M" ($\rho_M = \Sigma\, b_i/\Omega_M$)
R_g	Radius of gyration

RO-Membranes and desalination

RO-EC	Pressure cell without membrane
RO-MC	Pressure cell with membrane
PA	Polyamide (PA) selective layer
PSU	Polysulfone support layer
PP	Polypropylene, fabric layer
TFC	Thin Film Composite membrane
d_M	Thickness of membrane plus spacer
d_S	Channel height of the feed in RO-EC
$\Delta d_S = (d_S - d_M)$	Channel height of the feed in RO-MC
κ	Specific electrical conductivity
Λ_m	Molar conductivity
K	Kohlrausch coefficient
J_W	Permeate flux [L/(m^2 h)]
A	Permeability [L/(m^2 h bar)]
c_f	Salt concentration of the feed
π_f	Osmotic pressure of the feed
Φ	Osmotic coefficient
c_p	Salt concentration of the permeate
π_p	Osmotic pressure of the permeate
c_{mf}	Salt concentration of the feed at the membrane surface
π_{mf}	Osmotic pressure of the feed at the membrane surface
$\Delta\pi_{mf} =$	$(\pi_{mf} - \pi_p)$
Re	Reynolds number
CP	Concentration polarization
D_S	Solution diffusion coefficient in water
δ	Boundary layer thickness of CP
$k_f = D_S/\delta$	Mass transfer coefficient [m/s]
J_W/k_f	Peclet number

Appendix A. Operando Experiments

In the main text we have shown the data of neutron transmission and permeate flux as a function of pressure. Here we show the time behavior of the corresponding measurement data at a constant pressure of $\Delta P = 27$ bar to track the history of the feed concentration over a longer period.

A1. Permeate Flux, electrical Conductivity and Neutron Transmission of salt-free Water and $GdCl_3$ + NaCl solution

This section presents data from time-dependent experiments carried out at a pressure of 27 bar and a crossflow of 18 L/h. The permeate flux (J_W) and electrical conductivity (κ) of salt-free H_2O and a solution containing $GdCl_3$ and NaCl are shown in Figure A1(a) and (b), respectively. The flux of DI-H_2O reaches a stable value after about 10 h, while the salt solution does not reach a stable value even after 40 h of operation. The influence of crossflow was also tested in Figure A1(b), for the permeate flux as well as for the transmission in Figure A2(b). The κ in Figure A1(b) shows small oscillations around the control parameter of 7.5 mS/cm. Without the control of κ the concentration of the salts would continuously increase due to the permeate flux. Such an increase is prevented by feeding DI-H_2O into the circuit by means of a constant κ value of 7.5 mS/cm. Further details on the controlling system can be found in Ref. [10]. Figure A2 shows the time evolution of the corresponding transmission of the RO-MC and RO-EC cells with (a) DI-H_2O and (b) $GdCl_3$ + NaCl solutions at 27 bar. The data are stable after rapid equilibration. This means that the $GdCl_3$ concentration does not change, i.e. salt accumulation on the membrane surface is the only phenomenon observed.

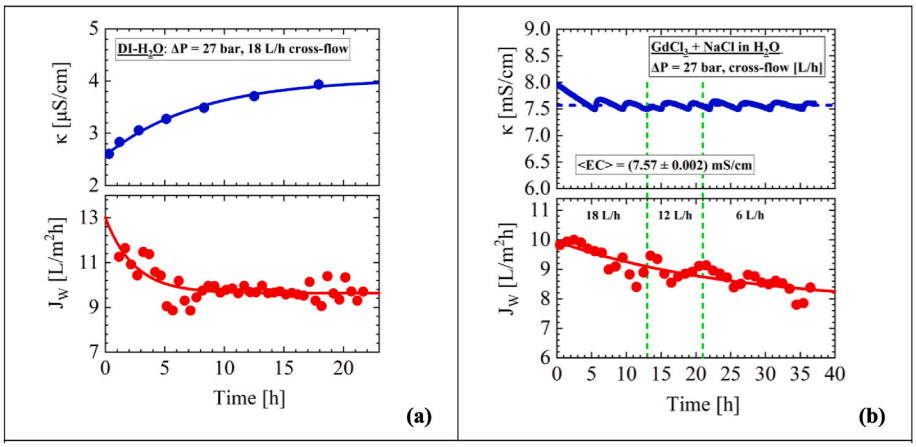

Fig. A1. **(a)** Electrical conductivity (κ) and permeate flux (J_W) of salt-free H_2O and **(b)** salt mixture of $GdCl_3$ and NaCl dissolved in DI-H_2O.

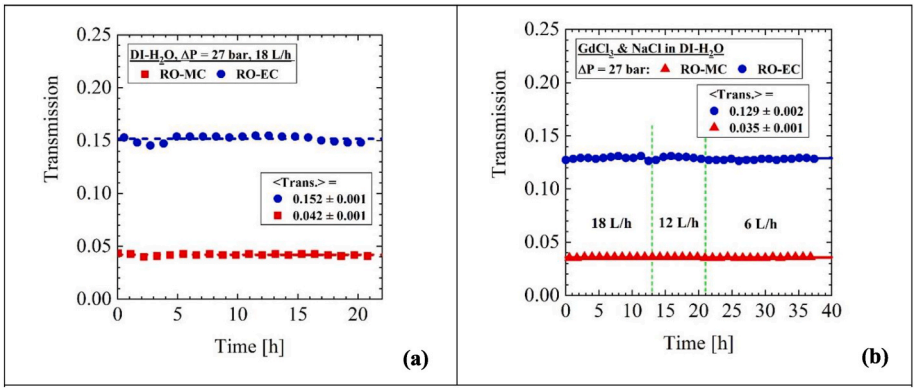

Fig. A2. Transmission of RO-MC and RO-EC cells with **(a)** DI-H_2O and **(b)** Solution of 1.06 g/L $GdCl_3$ + 4.69 g/L NaCl at the given conditions.

A2. Long duration Scattering Data ($d\Sigma/d\Omega(Q)$) of a $GdCl_3$ + NaCl Solution

In parallel with neutron transmission, the corresponding small-angle scattering (SANS) were also determined, which reveal the temporal behavior of the membrane pores of the two support layers, as described in detail in Ref. [14]. Figure A3(a)shows the scattering intensity as a macroscopic cross-section $d\Sigma/d\Omega(Q)$ in absolute units of cm^{-1} as a function of the momentum transfer Q measured at the time point after 13.2 h of the operando experiment together with the parameters and the radius of gyration (R_g) of the PSU and PP membrane support layers during a 40-h operando SANS experiment at 27 bar and variable crossflows of 18, 12 and 6L/h. The parameters $d\Sigma/d\Omega(0)$ and R_g in Figures A3(b) and (c) were obtained from fitting the scattering equation as elaborated in Ref. [14]. Within statistical uncertainty, the scattering data show no change over time, even though the crossflow was reduced from 18 L/h to 6 L/h in consistence with the data on membrane compaction in Ref. [15].

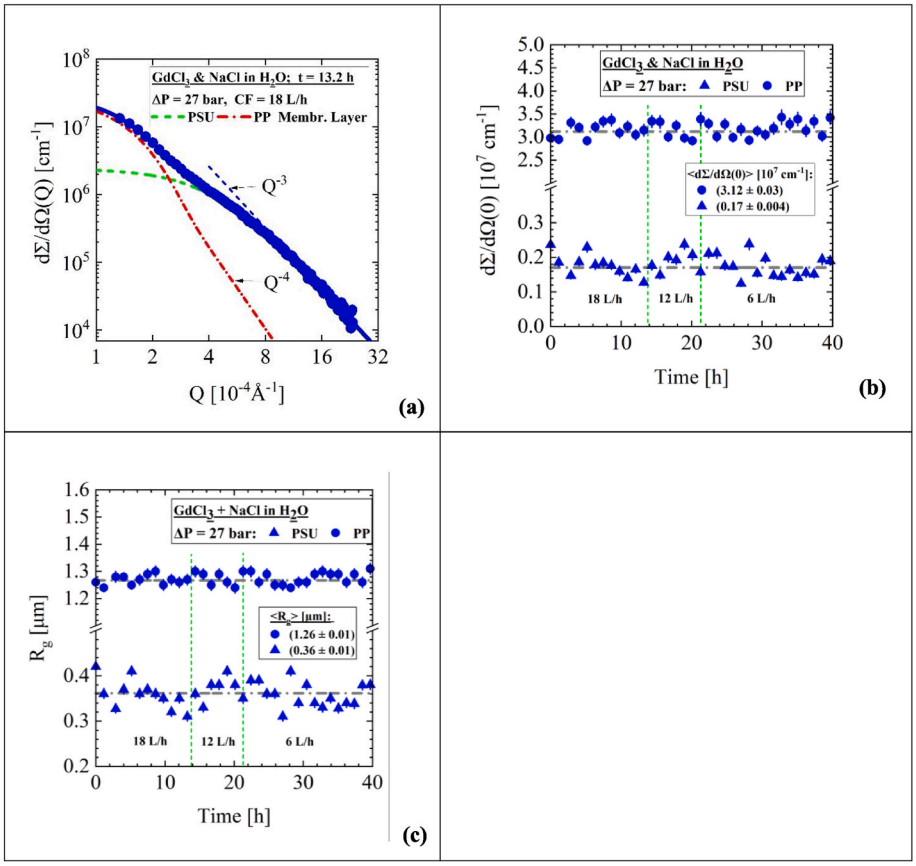

Fig. A3. **(a)** Scattering pattern of the RO98 pH t membrane. **(b)** and **(c)** show the corresponding parameters of the membrane scattering exposed to the $GdCl_3$ + NaCl aqueous solution feed.

The constant electrical conductivity (κ) over time (Figure A1(b)) and neutron transmission (Figure A2(b)) indicate a constant average $GdCl_3$ polarization of CP = (1.71 ± 0.09). This value represents the averaged value over the feeding height of the membrane, which is somewhat lower than the value observed in Fig. 6 for short-term CP = (1.97 ± 0.18) measurements. Only the permeate flux in Figure A1(b) shows a steady decrease from 10 to 8.4 L/(m^2 h), or 16 % (0.4 % per hour), over nearly 40 h.

Appendix B

Water permeation from aqueous Solutions of NaCl, $GdCl_3$, and their Mixture.

This section serves as an appendix to section 3.1. In the neutron transmission experiments, an aqueous mixture of NaCl and $GdCl_3$ was examined to determine the $GdCl_3$ concentrations in the feed far upstream and at the vicinity of the membrane surface (Fig. 6). A selective determination of the $GdCl_3$ concentration was possible due to the strong neutron absorption cross-section of Gd. As in the other experiments, these were accompanied by measurements of membrane permeability and electrical conductivity (Fig. 3). Here we show the results of further experiments on permeability for the individual salts and for their mixture at the nominal concentrations of 1.5 g/L $GdCl_3$ and 4.69 g/L NaCl, but without neutron transmission measurements. They were also carried out with the same equipment under the same external and hydrodynamic conditions as those with neutron transmission.

Fresh RO98 pHt membrane samples were used in these experiments. As shown in Figure B1 these membranes have higher permeability compared to the previous ones. Figure B1(a) shows the permeate flux of membrane sample 1 of DI-H_2O and the $GdCl_3$ solution, represented by blue spheres and red squares, respectively. Figure B1(b) shows the flux data of membrane sample 2 for DI-H_2O and the solutions with NaCl and $GdCl_3$ + NaCl. As shown, the permeability of membrane sample 2 for DI-H_2O is 65 % larger than that for membrane sample 1. In comparison to the permeate flux with the membrane used in the neutron experiment (Fig. 3(a)) even a 3 to 4 time increase in flux is observed for this new membrane batch, demonstrating relatively strong fluctuations in membrane properties within the same production batch. The electric conductivities, salt concentrations, permeabilities and the osmotic pressures $\Delta\pi_f$ of the salt solutions are compiled in Table 1. As mentioned in Appendix A the salt concentration had to be constantly checked by κ because of the continuous loss of salt-free water due to the permeate flux. This is the reason for the slightly increased salt content compared to the nominal values, resulting from the conductivity control. The osmotic pressure $\Delta\pi_f$ of the aqueous NaCl (4.69 g/L) solution is obtained from flux experiments in Figure B1(b) as $\Delta\pi_f(\text{NaCl}) = (1.95 \pm 0.56)$ bar. $\pi_f(\text{NaCl})$ as formulated in Eq. (C3) gives $\Delta\pi_f(\text{NaCl}) = 3.63$ bar [26]. The permeate has a NaCl concentration of 1.17 g/L, as can be seen from the chemical analysis in Table B1, which corresponds to a rejection rate of 74.5 % and leads to a $\pi_p = 0.91$ bar and thus a $\Delta\pi_f(\text{NaCl}) = 2.72$ (Fig. 4). This value is slightly larger than our experimental value.

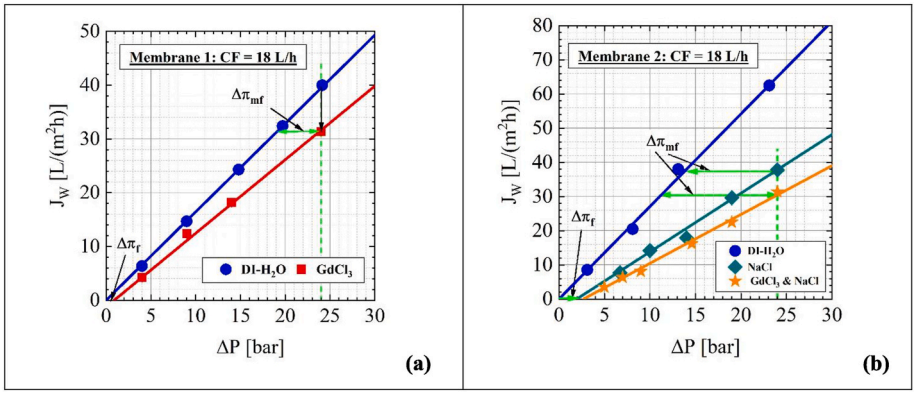

Fig. B1. Permeate flux results of the salt solutions together with DI-H_2O. (**a**) The flux of the $GdCl_3$ salt solution (red squares) depicted together with the DI-H_2O (blue dots) data were performed with membrane sample 1. **(b)** Shows the flux measurements of the NaCl and the mixture of NaCl + $GdCl_3$ solutions performed with membrane sample 2.

In Figure B2 the time dependence of the permeate flux measured at ΔP = 24 bar and CF = 18 L/h is shown. In our experience, the permeate flux generally follows an exponential law of the form. $J_W = J_{W,0} + A\exp(-t/\tau)$, as also observed in Figure A1(a) and in our previous Operando-SANS studies [14]. Of particular interest are the two flux data of the $GdCl_3$ solution in Figure B2 measured at ΔP = 24 bar and 12 L/h. The first measurement (blue sphere) was immediately started after completion of the preceding measurement at 24 bar and 24 L/h, while the second measurement (red triangle) was only started after the system had relaxed for about 5 min at ambient pressure and a CF of 12 L/h. The data of the first run shows a comparable low permeate flux with a slower decline with time to 28 L/(m^2 h). The data after flushing at 1 bar (red triangle) show an enhanced flux of more than 34 L/(m^2 h) followed by a fast decline to its steady state value of about 28 L/(m^2 h), very similar to the value of the first run. The development of CP is particularly marked by the time courses of J_W in Figures B2(b) and (c), as indicated by the black arrows starting at 34.5 L/(m^2 h) and 42.4 L/(m^2 h) near the flux of DI water at about 40 L/(m^2 h) (Figure B2(a)), i.e. at nearly zero CP. The concentrations of Na and Gd in the permeate as determined by ICP-OES are summarized in Table B1. This clearly shows that before starting a new experiment the prevailing CP layer in front of the membrane must be cleaned - here by flushing - before starting with changed parameter sets. The rejection with respect to the nominal salt concentrations of the feed is for Gd about 90 and 95 % at 20 and 10 bar, respectively, and for Na by about 74.5 % at ΔP = 24 bar, while for the salt mixture of NaCl and $GdCl_3$, both elements, Na and Gd, are rejected within 1 % to about 86 % [23]. Table B1 shows a $GdCl_3$ concentration in the permeate of about 10 % of the feed concentration. An estimate of the GdCl3 concentration in the membrane and the spacer results in a value of about 0.5 % of the corresponding feed volume fraction, which can safely be neglected.

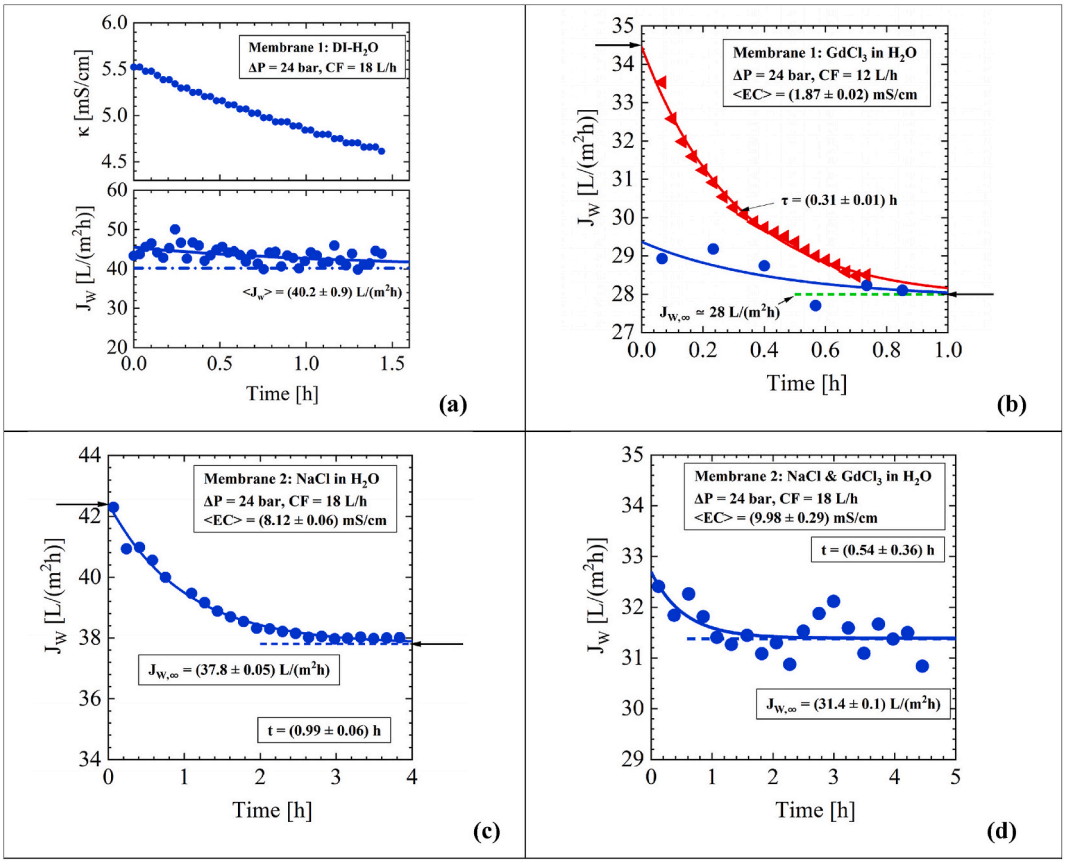

Fig. B2. Permeate flux measurements. **(a)** Compaction: J_W and κ at CF = 18 L/h versus time of deionized H_2O. **(b)** Start of experiment after: (1.) ΔP = 24 bar; CF = 24 L/h and (2.) ΔP = 0 bar; CF = 12 L/h, whereas **(c)** NaCl and **(d)** the mixture of NaCl + $GdCl_3$ were exposed to membrane sample 2 showing a larger permeability of about 65 %.

Table B1
Concentration of Na and Gd ions in the permeates and their rejection compared to the nominal salt concentrations [23].

Pressure [bar]		25	25	20	10	25		20	10
Nominal c [g/L] (Feed)		c [mg/L] (Permeate)				Rejection [%]			
NaCl (Na)	$GdCl_3$ (Gd)	Na	Gd			Na	Gd		
–	1.5 (1.2)	–	–	131.1 ± 1.1	64.4 ± 0.4	–	–	89.1	94.1
4.69 (2.98)	–	747 ± 13	–	–	–	74.9	–	–	–
4.69 (2.98)	1.5 (1.2)	402 ± 7	175.3 ± 1.3	–	–	86.5	85.4	–	–

Appendix C. Relevant Parameters for Analysis

C1. Effect of pressure on feed channel height (d_S) and membrane thickness as determined from the transmission of salt-free D_2O

The channel height (d_S) is a relevant parameter to determine the scattered neutron intensity in absolute units (Figure A3) and thereby determine the salt concentration from transmission. In particular, the dependence on pressure must be known. Figure C1(a) shows d_S of RO-EC plotted against pressure ΔP as determined from transmission of salt-free D_2O (Eq. (1)). D_2O is suited for this measurement because deuterium has a strong coherent but low incoherent scattering cross-section compared to hydrogen (2.05 and 80.27 b, respectively), i.e. good scattering signal and negligible multiple scattering.

The channel height of the cell for ambient pressure by cell design is $d_S = 0.136$ cm delivering $\Sigma(D_2O) = (1.42 \pm 0.01)$ cm^{-1} (Eq. (1)). The relevant height for the feed on top of the membrane is $\Delta d_S = (d_S - d_M)$ with the membrane plus spacer thickness of $d_M = 0.058$ cm at large ΔP (Figure C1(c)). The spacers are typically made of the same material as the fabric support layer. The mesh size of the spacer and the membrane have no influence on the determination of the $GdCl_3$ concentration from neutron transmission. This means that a constant crossflow of, for example, 18 L/h will exhibit a variation of the crossflow velocity with pressure due to the change in channel height, as shown in Figure C1(b).

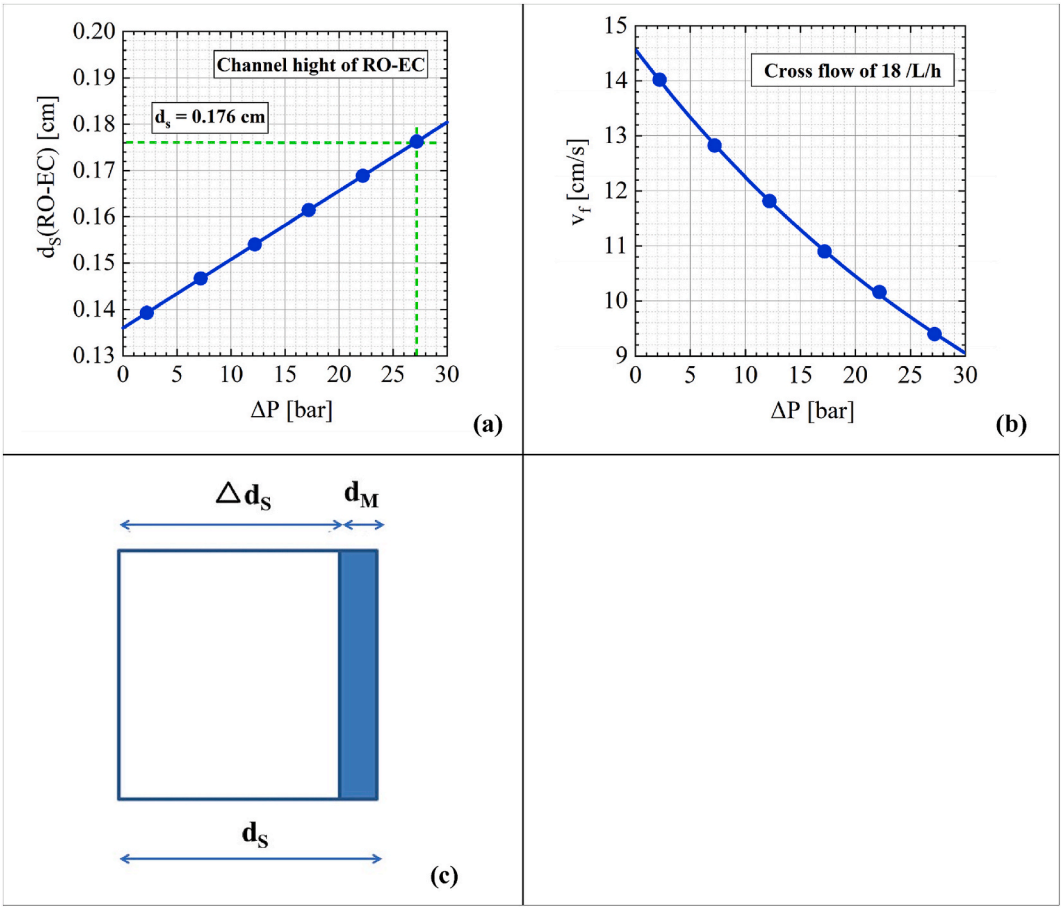

Fig. C1. **(a)** RO-EC channel height (d_S) versus pressure as determined from transmission of salt-free D_2O. Design and measurement at ambient pressure gives channel height $d_S = 0.136$ cm. **(b)** Crossflow velocity in [cm/s] of the feed above the membrane versus pressure of 18 L/h. **(c)** Dimensions of Alfa Laval RO-MC cell: Channel height of feed $\Delta d_S = (d_S - d_M)$ as well as the total thickness d_M of membrane and spacer shown as a blue area.

C2. Neutron relevant Parameters

Table C1 shows the interaction parameters of the $GdCl_3$ and NaCl salt molecules with neutrons such as the coherent scattering length density ρ and the macroscopic absorption cross-section Σ_{abs} [cm^{-1}] for the actual $\lambda = 12.8$ Å. The molecular Σ_{abs} is obtained from σ_{abs} divided by the volume of $GdCl_3$ and NaCl. The huge gadolinium absorption cross-section is the relevant property for the determination of low $GdCl_3$ concentrations in the order of 1 g/L or $\Phi = 0.22 \times 10^{-3}$ vol fraction [11].

Table. C1
Neutron relevant parameters of $GdCl_3$ and NaCl.

Molecule	Molar Mass [g/mol]	Mass density [g/cm^3]	Molar volume [cm^3/mol]	Solubility in H_2O [g/cm^3] (25 °C)	ρ [10^{10} cm^{-2}]	Σ_{abs} [cm^{-1}] ($\lambda = 12.8$ Å)
$GdCl_3$	263.61	4.52	58.32	0.95×10^{-2}	4.016	**3.68×10^3**
NaCl	58.44	2.16 (25 °C)	27.06	0.36×10^{-2}	2.94	**5.42**

C3. Relevant Parameters from Literature of the Salt Concentrations, electric Conductivity, and Osmotic Pressure

To determine the salt concentrations, we need the relationship of the electrical conductivity (κ) of aqueous $GdCl_3$ and NaCl as a function of their salt concentration, which we have taken from the literature [24] ($GdCl_3$) and [25,26] (NaCl) and which are plotted in Figure C2. Since κ is not known for $GdCl_3$ at the low concentrations of 1.06 and 1.5 g/L, we have determined the required values by extrapolation using the Kohlrausch equation in Eq. (C1). The calculated results for $GdCl_3$ and NaCl according to the Kohlrausch equation are shown in Figure C2(a). Λ_m describes the molar electrical conductivity ($\Lambda_m = \kappa / C$) of strong electrolytes well for low concentrations [25]. The units of the conductivity and of the molar conductivity are [κ] = mS/cm and [$\Lambda_m = \kappa / C$] = (mS/cm)/mM), respectively. The Kohlrausch coefficient [K] = $(mS/cm)/(mM)^{3/2}$ mainly depends on the stoichiometry of the specific salt in solution [27]. The conductivities in Figure C2(b) were fitted with $\kappa = \Lambda_m^0 C - K C^{3/2}$ showing the κ of the nominal 4.02 mM and 5.69 mM $GdCl_3$ and 80.3 mM NaCl salt solutions as arrows and summarizes all parameters from the fits in Table C2. For comparison, the transmission data, i.e. the concentration of $GdCl_3$ from transmission measurements (Fig. 6(a)) and from the electric conductivity of the two salts (Fig. 3(b)) are shown in Table C2. The κ of both salts determined by Kohlrausch for the conditions of the neutron experiments is (9.7 ± 0.5) mS/cm and is about 20 % larger than the value of (8.10 ± 0.07) mS/cm determined by the neutron experiments.

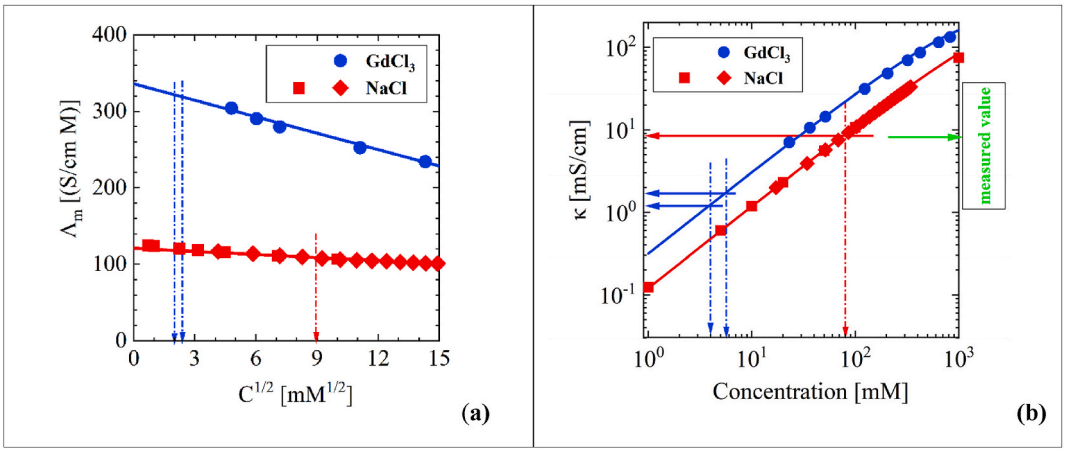

Fig. C2. **(a)** Molar conductivity Λ_m of aqueous $GdCl_3$ (blue sphere Supporting information Table II [24]) and of NaCl (red square p. 30, Tables 2–2 [25]) and [26] (red rhombus) as a function of the square root of concentration. The data in the diagram were fitted using the Kohlrausch function Eq. (C1) and in **(b)** using the expression $\kappa = \Lambda_m^0\, C - K\, C^{3/2}$ discussed in the text. The green arrow indicates the experimental conductivity of the electrolytic solution.

$$\Lambda_m = \Lambda_m^0 - K\sqrt{C} \tag{C1}$$

Table C2
Electrolyte concentration and conductivity of aqueous $GdCl_3$ and NaCl at T = 25 °C and the concentrations c and C of our samples from neutron transmission and literature [24–26].

Molecules		c nominal	C nominal	c Fig. 6(a)	Λ_m^0	K (Kohlrausch)	κ	κ Fig. 3(b)
		[g/L]	[mM]	[g/L]	[(S/(cm M)]	[(mS/cm)/(mM)$^{3/2}$]	[mS/cm]	[mS/cm]
$GdCl_3$	Section 3	1.06	4.02	(1.05 ± 0.04)	334 ± 4	- (7.17 ± 0.5)	1.28 ± 0.05	
	Appendix B	1.5	5.69				1.80 ± 0.05	
NaCl		4.69	80.3	–	126 ± 0.2	- (2.33 ± 0.06)	8.43 ± 0.33	
$GdCl_3$ + NaCl				–			9.7 ± 0.5	8.10 ± 0.07

The osmotic pressure (π_f) in Eq. (4) is described by a modified van't Hoff equation displayed in Eq. (C2). The osmotic pressure is proportional to the number of dissociating ions (i), the osmotic coefficient (Φ), the salt concentration c in [g/L], the gas constant (R), and absolute temperature (T), and is inversely proportional to the molecular weight M_W in [g/mol] [26]. This reference gives π_f of a NaCl aqueous solution as a function of concentration (c) in [g/L] as shown in Eq. (C3) and depicted in Figure C3. An osmotic pressure of $\pi_f(NaCl) = 3.63$ bar is evaluated for 4.69 g/L NaCl solution and a $\Delta\pi_f(NaCl) = 2.69$ bar if considering a rejection rate of 74.5 % as determined from chemical analysis in Table B1. The experimental value from flux experiment in Figure B1(b) and Table 1 determined a slightly smaller value of $\Delta\pi_f(NaCl) = (1.95 \pm 0.56)$ bar, whereas the SANS data shows with $\Delta\pi_f = (2.19 \pm 0.15)$bar (Fig. 3(a) and Table 1) a value in between.

$$\pi_f = i\ \Phi\ c\ R\ T\ /\ M_W \tag{C2}$$

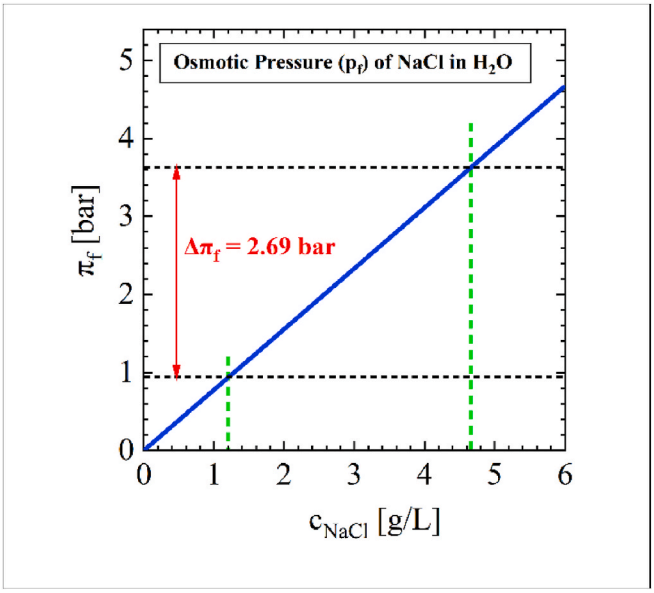

Fig. C3. Osmotic pressure π_f of NaCl versus concentration determined from Ref. [24]. $\Delta\pi_f(NaCl)$ determined from π_f of the nominal NaCl concentration of 4.69 g/L ($\pi_f = 3.63$ bar) and of the 25.5 % NaCl concentration of the effluent of 1.19 g/L (Table B1) delivering $\pi_f = 0.943$, thereby giving a $\Delta\pi_f = 2.69$ bar.

$$\pi_f(\mathrm{NaCl}) = \mathrm{K}\,\Phi(c)\,c = 0.848 \times \left(3.14 \times 10^{-6}\,c^2 + 2.13 \times 10^{-4}\,c + 0.917\right) \times c \quad \text{(C3)}$$

C4. Determination of the Reynolds Number

The crossflow of 18 L/h corresponds to crossflow velocities between 14.6 and 9.4 cm/s based on the channel thickness for the hydrostatic pressure ΔP between 0 and 27 bar (Figure C1). Under these conditions, laminar flow prevails, as the largest Reynolds number of Re = 216 is smaller than the critical Re number, which is given in the literature as 2320 for smooth round pipes. The Reynolds number defined as $Re = v \times L / \mu$ is proportional to the crossflow velocity v and the characteristic length L interpreted as the hydraulic diameter ($L = 2\,(a \times b)/(a + b)$, a = 4.5 cm, b = 0.118 cm at 27 bar) of 0.23 cm, and inversely proportional to the kinematic viscosity of water given as $\mu = 1.002 \times 10^{-2}$ cm^2/s at 20 °C.

Data availability

Data will be made available on request.

References

[1] M.E. Williams, A brief review of reverse osmosis membrane technology. https://www.academia.edu.

[2] M. Qasim, M. Badrelzaman, N.N. Darwish, N.A. Darwish, N. Hilal, Reverse osmosis desalination: a state-of-the-art review, Desalination 459 (2019) 59–104, https://doi.org/10.1016/j.desal.2019.02.008.

[3] A. Matin, F. Rahman, H.Z. Shafi, S.M. Zubair, Scaling of reverse osmosis membranes used in water desalination: phenomena, impact, and control; future directions, Desalination 455 (2019) 135–157.

[4] W. Bai, L. Samineni, P. Chirontoni, I. Krupa, P. Kasak, A. Popelka, N.B. Saleh, M. Kumar, Quantifying and reducing concentration polarization in reverse osmosis systems 554 (2023) 116480.

[5] O. Jung, F. Saravia, S. Heißler, H. Horn, Quantifying concentration polarization – raman microspectroscopy for *In-Situ* measurement in a flat sheet cross-flow nanofiltration membrane unit, Sci. Rep. 9 (2019). Article number: 15885.

[6] J. Fernández-Sempere, F. Ruiz-Beviá, P. García-Algado, R. Salcedo-Díaz, Experimental study of concentration polarization in a crossflow reverse osmosis system using digital holographic interferometry, Desalination 257 (2010) 36–45.

[7] B. Meng, X. Li, In situ visualization of concentration polarization during membrane ultrafiltration using microscopic laser-induced fluorescence, Environ. Sci. Technol. 53 (2019) 2660–2669.

[8] M. Zargar, R. Ujihara, S.J. Vogt, J.S. Vrouwenvelder, E.O. Fridjonsson, M.L. Johns, Imaging of membrane concentration polarization by NaCl using ^{23}Na nuclear magnetic resonance, J. Membr. Sci. 600 (2020) 117868.

[9] D.L. Shaffer, J.M. LaManna, D.L. Jacobson, D.S. Hussey, M. Elimelech, E.P. Chana, Forward osmosis studying water and solute transport through desalination membranes via neutron radiography, J. Membr. Sci. 548 (2018) 667–675, https://doi.org/10.1016/j.memsci.2017.10.046.

[10] V. Pipich, Th Starc, J. Buitenhuis, R. Kasher, W. Petry, Y. Oren, D. Schwahn, Silica fouling in reverse osmosis systems–operando small-angle neutron scattering studies, Membranes 11 (2021) 413, https://doi.org/10.3390/membranes11060413.

[11] V.F. Sears, Neutron scattering lengths and cross sections, Neutron News 3 (1992) 26–37.

[12] Heinz maier-leibnitz-zentrum. http://www.mlz-garching.de/instrumente-und-labore/nanostrukturen/kws-3.html.

[13] KWS-3: Very small-angle scattering diffractometer with focusing mirror, Journal of large-scale research facilities, 1, A31. https://doi.org/10.17815/jlsrf-1-28.

[14] V. Pipich, M. Dickmann, H. Frielinghaus, R. Kasher, Ch Hugenschmidt, W. Petry, Y. Oren, D. Schwahn, Morphology of thin film composite membranes explored by small-angle neutron scattering and positron-annihilation lifetime spectroscopy, Membranes 10 (2020) 48, https://doi.org/10.3390/membranes10030048.

[15] V. Pipich, Th Starc, R. Kasher, W. Petry, Y. Oren, D. Schwahn, The porous system of RO membrane supporting layers - operando studies with small-angle neutron scattering, Chem. Eng. J. 495 (2024) 153304.

[16] V. Pipich, K. Schlenstedt, M. Dickmann, R. Kasher, J. Meier-Haack, Ch Hugenschmidt, W. Petry, Y. Oren, D. Schwahn, Morphology and porous structure of standalone aromatic polyamide films as used in RO membranes – an exploration with SANS, PALS, and SEM, J. Membr. Sci. 573 (2019) 167–176.

[17] S. Whitaker, Flow in porous media I: a theoretical derivation of Darcy's law, Transport Porous Media 1 (1986) 3–25.

[18] D.B. Dorhjie, R. Yusupov, V. Krutko, A. Cheremisin, Deviation from darcy law in porous media due to reverse osmosis: pore-scale approach, Energies 15 (2022) 6656.

[19] R.W. Baker, Membrane Technology and Applications, fourth ed., *John Wiley & Sons*, 2023, 978-1-119-68598-2.

[20] E.S. Jang, W. Mickols, R. Sujanani, A. Helenic, T.J. Dilenschneider, J. Kamcev, D. R. Paul, B.D. Freeman Paul, Influence of concentration polarization and thermodynamic non-ideality on salt transport in reverse osmosis membranes, J. Membr. Sci. 572 (2019) 668–675, https://doi.org/10.1016/j.memsci.2018.11.006.

[21] T.Y. Qiu, P.A. Davies, Concentration polarization model of spiral-wound membrane modules with application to batch-mode RO desalination of brackish water, Desalination 368 (2015) 36–47, https://doi.org/10.1016/j.desal.2014.12.048.

[22] E. Lyster, Y. Cohen, Numerical study of concentration polarization in a rectangular reverse osmosis membrane channel: permeate flux variation and hydrodynamic end effects, J. Membr. Sci. 303 (2007) 140–153, https://doi.org/10.1016/j.memsci.2007.07.003.

[23] The Chemical Analysis Was Carried out at the Central Institute of Engineering, Electronics and Analytics (ZEA-3) of the Forschungszentrum Jülich Gmbh, D-52425 Jülich.

[24] F.H. Spedding, J.A. Rard, V.W. Saeger, Electric conductances of some aqueous rare Earth electrolyte solutions at 25 °C. II. Rare Earth chlorides, J. Chem. Eng. Data 19 (4) (1974) 373–378 (Supporting information, Table II).

[25] C.H. Hamann, W. Vielstich, Elektrochemie I, Verlag Chemie, Weinheim, 1985.

[26] Downloaded from Horiba (Water & Liquids).

[27] P.W. Atkins, The Elements of Physical Chemistry, *third ed.*, *Oxford University Press*, 2001, 0-19-879290-5.